Rapid Communications

Optical-lattice-based Cs active clock with a continual superradiant lasing signal

Duo Pan,[1] Bindiya Arora,[2] Yan-mei Yu,[3,4,*] B. K. Sahoo,[5,†] and Jingbiao Chen[1,‡]

[1]*State Key Laboratory of Advanced Optical Communication Systems and Networks, Department of Electronics, Peking University, Beijing 100871, China*

[2]*Department of Physics, Guru Nanak Dev University, Amritsar, Punjab 143005, India*

[3]*Beijing National Laboratory for Condensed Matter Physics, Institute of Physics, Chinese Academy of Sciences, Beijing 100190, China*

[4]*University of Chinese Academy of Sciences, 100049 Beijing, China*

[5]*Atomic, Molecular and Optical Physics Division, Physical Research Laboratory, Navrangpura, Ahmedabad 380009, India*

(Received 3 March 2020; accepted 29 September 2020; published 21 October 2020)

We demonstrate the state-of-the-art technique of an active clock to provide a continuous superradiant lasing signal using an ensemble of trapped Cs atoms in an optical lattice. A magic wavelength of the proposed $|7S_{1/2}; F = 4, M_F = 0\rangle \rightarrow |6P_{3/2}; F = 3, M_F = 0\rangle$ clock transition in Cs atoms is identified at 1181 nm for constructing the optical lattice. Pertinent optical lines are also found for pumping and repumping atoms from their ground states. A fractional uncertainty about 10^{-15} in the clock frequency has been predicted by carrying out rigorous calculations of several atomic properties. The bad-cavity operational mode of the active clock is anticipated to improve remarkably its short-term stability by suppressing intrinsic thermal fluctuations. Thus, a composite clock system with better short-term and long-term stabilities can be built by combining the proposed active clock with another high-accuracy passive optical clock.

DOI: 10.1103/PhysRevA.102.041101

It is well known that, owing to its natural immunity against the cavity thermal noise floor, hydrogen masers offer better instability among the microwave atomic clocks within the first 30 seconds of frequency measurement, referred to as its short-term stability. In contrast, passive clocks, whose operations rely mainly on the local oscillators and reference cavities, suffer from the degeneration of the short-term stability caused by the instability of the local oscillators and thermal noise of the reference cavities. The short-term instabilities of the local oscillators of the currently running passive clocks are now as low as 4×10^{-17} at 1 s by decreasing thermal noise through cryogenic optical cavities [1–3]. To overcome this limitation, it has prompted many people to develop techniques to attain improved short-term stabilities in atomic clocks [4–9]. In the quest of achieving better short-term stability in an optical clock, we demonstrate here a proof of principle to build up an active optical clock by adopting a similar working principle as a hydrogen maser [10–15]. The underlying principle of an active optical clock lies in its robustness to infer the clock frequency directly from the superradiant signal of an ensemble of atoms placed inside a "bad-cavity." In principle, the active optical clock can achieve short-term instabilities well below the cavities thermal noise limit and at the same time it can relax the requirement for the cryogenic ultrastable cavity, thus reducing the systematic complexity. The short-term stabilities of these clocks can be improved appreciably by suppressing photon shot noise through continuous pumping and output lasing signals. The previously proposed two-level active optical clocks [13,14] are compelled to produce signals intermittently to overcome interference between the applied pumping pulse with the output clock lasing signal. The stability and accuracy of continuous signal production proposed in a three-level clock [10] are critically obstructed by the light shift caused by the pumping laser. To explore in this direction further, we analyzed four atomic levels accessible by optical lasers in an ensemble of thermal Cs atoms for a possible continuous signal production active optical clock in Ref. [16]. However, this is also subjected to large systematics due to light shifts and collisional decoherence.

In this work, we expound on the feasibility of an active optical clock using four suitable hyperfine levels of trapped cold Cs atoms, instead of the atomic energy levels of thermal Cs atoms proposed in Ref. [16], in a red-detuned one-dimensional (1D) optical lattice at a magic wavelength λ_m of the $|7S_{1/2}; F = 4, M_F = 0\rangle \rightarrow |6P_{3/2}; F = 3, M_F = 0\rangle$ clock transition. The schematic layout of our experimental setup and the associated hyperfine levels are shown in Figs. 1(a) and 1(b), respectively. The unique advantages of adopting this technique with appropriate choices of hyperfine levels are at least threefold over the previous active optical clocks: it moderates interference between the pumping laser and the superradiant lasing signal, minimizes light shifts and collisional decoherence to the hyperfine levels, and provides sufficient time to conduct the experiment meticulously due to strong confinements of atoms in the optical lattice. A sufficiently weak magnetic field of about $\mathcal{B} = 10^{-7}$ T is applied to break the M_F degeneracy of the clock transition and a π-polarized pumping laser is locked at 455 nm for

*ymyu@aphy.iphy.ac.cn
†bijaya@prl.res.in
‡jbchen@pku.edu.cn

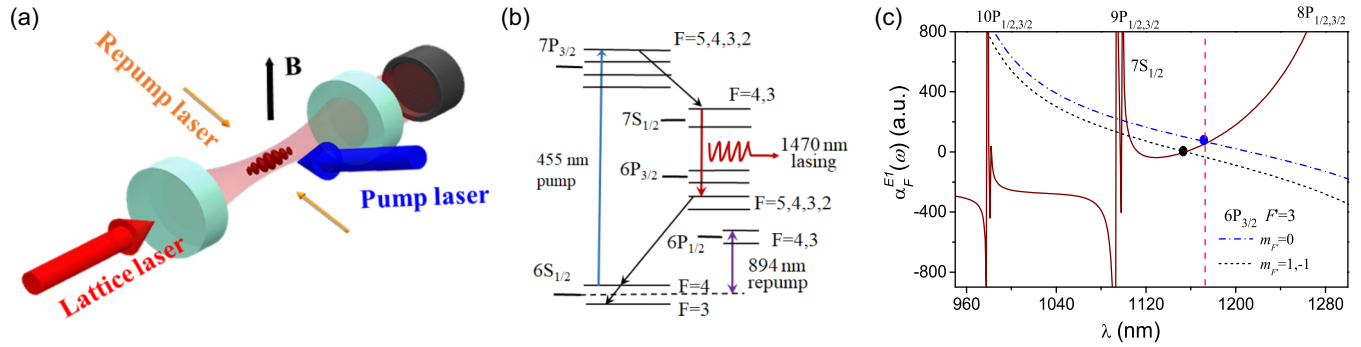

FIG. 1. Schematic depictions of (a) the experimental setup, in which cold Cs atoms are held in an 1D optical lattice situated inside a high-finesse cavity near magic wavelength λ_m of the $|7S_{1/2}; F = 4, M_F = 0\rangle \rightarrow |6P_{3/2}; F = 3, M_F = 0\rangle$ clock transition of the proposed four-level active clock, (b) the relevant energy levels for clock pumping and repumping transitions, and (c) a plot for $\alpha_F^{E1}(\omega)$ values (in a.u.) of the clock levels against wavelength λ (in nm) to infer required λ_m. Resonance lines for the $7S_{1/2}$ state are marked at the top of the plot.

populating Cs atoms to the $|7P_{3/2}; F = 5, M_F = 0\rangle$ level from the $|6S_{1/2}; F = 4, M_F = 0\rangle$ level of the ground state. Subsequently, these atoms decay to any of the $M_F = -1$, 0, or 1 sublevels of the $F = 4$ hyperfine level of the $7S_{1/2}$ state through spontaneous emission. At the same time, a bad-cavity mode is adjusted to couple with the clock transition, which is further locked to a supercavity [16]. The objective of this step is to attain self-gaining stimulated emission from the above transition in the bad-cavity mode and produce superradiant lasing. A polarization selector inside the cavity (not shown in the figure) helps to establish a superradiant lasing signal in the above transition through the allowed $(M_F \rightarrow M_F) \equiv (0 \rightarrow 0)$, $(1 \rightarrow 1)$, and $(-1 \rightarrow -1)$ decay channels. Then, atoms come down to either of the $F = 3$ or $F = 4$ hyperfine levels of the ground state. A 894 nm laser is applied at this stage to repump the atoms from all other magnetic sublevels to the desired $|6S_{1/2}; F = 4, M_F = 0\rangle$ level of the ground state by using a dual laser [17]. The combined pumping action, spontaneous emission, superradiant emission, and spontaneous decay channels follow the path of the $6S_{1/2} \rightarrow 7P_{3/2} \rightarrow 7S_{1/2} \rightarrow 6P_{3/2} \rightarrow 6S_{1/2}$ transitions successively to populate the $|6S_{1/2}; F = 4, M_F = 0\rangle$ level at the end of a complete cycle to perpetuate a continuous loop of clock operation. There is a probability that a fraction of atoms can populate the $5D_{3/2}$ and $5D_{5/2}$ states through spontaneous emission from the $7P_{3/2}$ state, but they will decay to the $6P_{1/2}$ and $6P_{3/2}$ states within 0.1 μs. Thus, the superradiant lasing is not going to be affected by such a process. Since interferences between the (re)pumping laser and the clock lasing signal do not occur in this procedure, a continuous signal of superradiant lasing at 1470 nm can be achieved.

An essential feature of our proposed experimental technique is to trap Cs atoms at a λ_m of the clock transition in an optical lattice. The most convenient choice is to use a π-polarized laser for creating a trapping potential, which can cause the AC-Stark shift in a hyperfine $|F, M_F\rangle$ level of atomic state as $\Delta E_F(\omega) = -\frac{1}{4}\alpha_F^{E1}(\omega)\mathcal{E}^2$ with amplitude of electric field $\mathcal{E}$ of trapping laser and dynamic electric-dipole ($E1$) polarizability of hyperfine level $\alpha_F^{E1}(\omega)$ for laser frequency ω. The $\alpha_F^{E1}(\omega)$ values of the hyperfine levels of the $7S_{1/2}$ and $6P_{3/2}$ clock states are determined by calculating their atomic-state polarizability $\alpha_J^{E1}(\omega)$ using the same method as in Refs. [18,19]. For this purpose, we have used the experimental energies and $E1$ matrix elements either from the literature [20–22] or by calculating them using a relativistic all-order method [23]. Uncertainties in the α_F^{E1} values are determined from the accuracies of the $E1$ matrix elements. The λ_m values of a transition corresponds to its null differential $\alpha_F^{E1}(\omega)$ values. We plot the $\alpha_F^{E1}(\omega)$ values of the hyperfine levels of the $7S_{1/2}$ and $6P_{3/2}$ states in Fig. 1(c) for the optical range of 950–1300 nm to locate possible λ_m values. The intersections of the polarizability curves mark the presence of a suitable λ_m at 1181 nm. The inferred $\alpha_J^{E1}(\omega)$ values of different states at $\lambda_m = 1181$ nm are quoted in atomic units (a.u.) in Table I. At 1181 nm, α_F^{E1} is 73(10) a.u. for the $7S_{1/2}$, $F = 4$ upper clock state, and $\alpha_F^{E1} = 73(36)$ a.u. for the $6P_{3/2}$, $F = 3$ lower clock state, as determined by its scalar and tensor α_J^{E1} values of $-381(32)$ a.u. and 629(13) a.u., respectively.

The 455 nm pumping laser can populate Cs atoms from the ground state to the excited state, simultaneously, the 894 nm repumping laser is used for Sisyphus cooling. The temperature of the trapped cold Cs atoms is determined by balancing the heating rate and the cooling effect; $k_B T_c = (D_p + D'_p)/\alpha_{cool}$, where D_p and D'_p are the momentum diffusion coefficients of the pumping and repumping lasers, respectively, and α_{cool} is the cooling coefficient due

TABLE I. Properties of Cs atoms and optical trap at 1181 nm magic wavelength. Here, τ, α_J^{E1}, and ρ represent natural lifetimes, atomic dipole polarizabilities, and populations, respectively, of investigated states in Cs atoms, while U_0, Γ_{sc}, and τ_L correspond to trapping potential, scattering rate, and lifetimes of atomic states due to the scattered photons, respectively, in the 1D optical lattice for the operational laser intensity $I_{op} = 20$ kW/cm^2. Uncertainties to the α_J^{E1} values are quoted explicitly, which are used for estimating the clock frequency shift.

State	τ (μs)	α_J^{E1} (a.u.)	U_0 (kHz)	ρ (%)	Γ_{sc} (kHz/s)	τ_L (s)
$6S_{1/2}$	∞	846(11)	-2957	27.1	2.6	1137
$5D_{5/2}$	1.37	793(38)	-2772	33.9	21.5	129
$5D_{3/2}$	0.97	730(37)	-2551	3.1	13.0	196
$7P_{3/2}$	0.11	8045(4388)	-28119	24.1	0.1	$>10^5$
$7S_{1/2}$	0.05	73(10)	-255	5.5	0.3	850
$6P_{3/2}$	0.03	$-381(32)$	-255	2.7	6.8	38

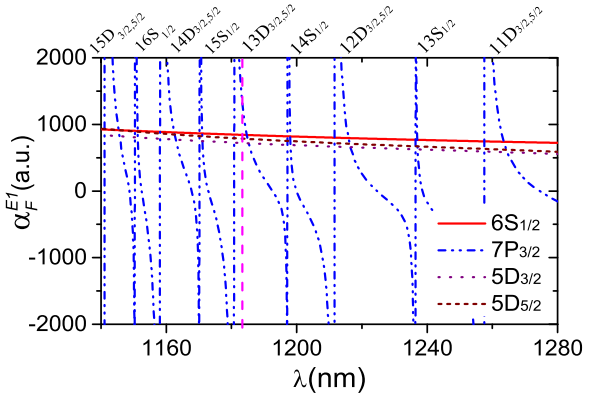

FIG. 2. Plot for $\alpha_F^{E1}(\omega)$ values (in a.u.) of hyperfine levels used for pumping and repumping transitions against wavelength (in nm). Resonance lines of the $7P_{3/2}$ state are labeled on the top of the plot. The dashed line shows the position of the λ_m value (i.e., 1181 nm) for the optical lattice.

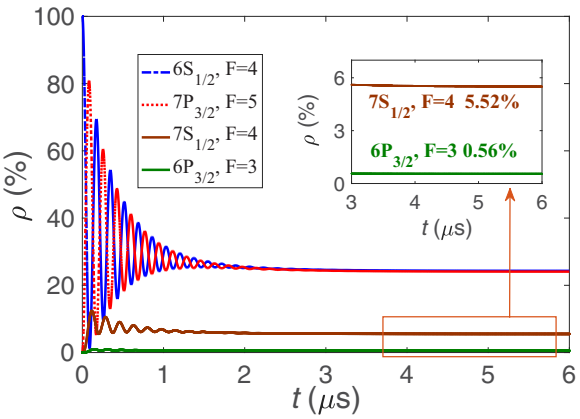

FIG. 3. Steady-state atomic populations ρ (in %) in different levels over a range of timescale t (in μs). Lattice, pumping, and repumping lasers are π polarized, and the lattice laser is adjusted to be resonating with a mode of cavity.

to the 894 nm laser. It yields $D_p = \frac{1}{2}\hbar^2 k^2 \Gamma_{455} = 1.9 \times 10^{-48}$ kg^{2}m^2/s^3 [24] with the Rabi frequency $\gg\Gamma_{455}$, wherein k and Γ_{455} are the wave vector and spontaneous decay rate, respectively, of the pumping transition and $\hbar$ is the Planck constant. We estimate $D_p' = 9.1 \times 10^{-48}$ kg^{2}m^2/s^3 for a repumping laser intensity of 2 mW/cm^2 and detuning $\delta = 30$ MHz using the formula $D_p' = (7/10)\hbar^2 k'^2 \Gamma_{894} s_0 + (3/4)\hbar^2 k'^2 (\delta^2/\Gamma_{894}) s_0$ [25,26], where $s_0 = \frac{\Omega^2/2}{\delta^2 + \Gamma_{894}^2/4}$ is the saturation parameter, wave vector k', Rabi frequency Ω, and spontaneous decay rate Γ_{894} of the repumping transition. Similarly, $\alpha_{cool} = 29\hbar^2 k'^2 \Gamma_{894}/(50 k_B T_0) = 2.2 \times 10^{-20}$ kg/s is obtained by using the reported Sisyphus cooling temperature $T_0 = 30\ \mu K$ [27]. Accounting for the above parameters, it yields the cooling temperature of the system $T_c = 35\ \mu$K, which is low enough to ensure effective loading of Cs atoms into the lattice.

The dipole potential of the 1D red-detuned optical lattice is constructed following Ref. [28]. The maximum trapping depth at the antinode position of the lattice is determined by $U_0 = -\alpha_F^{E1}(\omega)\mathcal{E}^2$ with $\mathcal{E} = \sqrt{2I/(c\epsilon_0)}$, where c and ϵ_0 are the speed of light and vacuum permittivity, respectively, and I is the average intensity of the laser. The strength of the trapping potential is gauged by investigating the $\alpha_F^{E1}(\omega)$ values for the corresponding hyperfine levels of the considered states at $\lambda_m = 1181$ nm. The $\alpha_F^{E1}(\omega)$ values of the levels associated with the pumping and repumping transitions are plotted for the wavelength range from 1140 to 1280 nm in Fig. 2. Using the $\alpha_F^{E1}(\omega)$ values, calculated in the same procedure as in Refs. [18,19], gives U_0 for the $6S_{1/2}$, $5D_{3/2}$, and $5D_{5/2}$ states, using a typical operational lattice intensity $I_{op} = 20$ kW/cm^2, three times larger than the thermal kinetic energy $k_B T$ of the trapped atoms at the estimated temperature $T \approx 35\ \mu$K and Boltzmann constant k_B. Due to the presence of a large number of resonant lines, it was strenuous to predict definite signs of $\alpha_F^{E1}(\omega)$ of the $7P_{3/2}$ state around $\lambda_m = 1181$ nm. Also, the U_0 values for the $7S_{1/2}$ and $6P_{3/2}$ states turn out to be quite small. Nonetheless, atoms will decay from these states to the $6S_{1/2}$, $5D_{3/2}$, and $5D_{5/2}$ states within tens of nanoseconds before they can escape from the lattice.

Since it is imperative to operate the optical lattice at a very low sensitivity against variation in the trapping laser wavelength to minimize fluctuation in the clock frequency, we estimate the rate of change in the clock frequency with respect to deviation in wavelength per unit power of the trapping laser. This comes out to be of the order of 0.7 Hz/[GHz (kw/cm^2)] around $\lambda_m = 1181$ nm from Fig. 1(c). By assuming a typical experimental condition of maximum 100 kHz deviation in the trapping laser frequency [29], the fractional clock frequency shift is expected to be about 6.9×10^{-18} for a typical value of $I_{op} = 20$ kW/cm^2.

The steady-state atomic populations in the investigated four levels of Cs atom during the clock frequency measurement are obtained by considering atom-pumping laser interactions in the Liouville or von Neumann equation, given by [30]

$$\frac{d\rho}{dt} = \frac{1}{i\hbar}[H_{AP}, \rho] - \frac{1}{2}\{\Gamma, \rho\}, \tag{1}$$

where $H_{AP} = H_{AP}^0 + H_{AP}^I$ is the total Hamiltonian comprising of the unperturbed Hamiltonian describing the upper ($|F_u, M_{F_u}\rangle$) and the lower ($|F_l, M_{F_l}\rangle$) levels of the pumping (or repumping) transition as $H_{AP}^0 = \sum_{i=u,l} E_{F_i} |F_i, M_{F_i}\rangle\langle F_i, M_{F_i}|$ with the eigenvalues E_{F_i} in the absence of laser field and interaction Hamiltonian $H_{AP}^I = -\frac{i}{\hbar}[\Omega_{F_l F_u} |F_l, M_{F_l}\rangle\langle F_u, M_{F_u}| + \Omega_{F_u F_l} |F_u, M_{F_u}\rangle\langle F_l, M_{F_l}|]$ with the Rabi frequencies $\Omega_{F_l F_u} = \Omega_{F_u F_l} = |\langle F_l \| D \| F_u\rangle| \mathcal{E}/\hbar$ for the field strength $\mathcal{E}$. We have used experimental values of energies and transition rates [31,32] to predict the atomic populations, which are shown in Fig. 3 for all the hyperfine levels of the above states and quoted explicitly in Table I by taking the pumping and repumping powers 500 mW/cm^2 and 2 mW/cm^2, respectively.

We also present the estimated lifetime τ_L and photon-scattering rate Γ_{sc} values in Table I. The lifetime of an atomic state in the far-detuned optical lattice trap due to photon scattering is estimated by $\tau_L = U_0/\Gamma_{sc}$, and the photon-scattering rate Γ_{sc} can be formulated as

$$\Gamma_{sc} = \frac{1}{6(2J_n + 1)} \sum_k \frac{|\langle J_n \| D \| J_k\rangle|^2}{(\hbar\omega_L - \delta E_{nk})^2} \Gamma_k \mathcal{E}^2, \tag{2}$$

where Γ_k is the spontaneous decay rate from the upper state k to the lower state n, and ω_L is the lattice laser frequency. As can be seen, the τ_L values are at least a few tens of seconds for different states, among which the $6P_{3/2}$ state has the shortest lifetime. This is still long enough for continuous operation of the clock.

The output power of the superradiant laser in the atom-cavity coupled system is determined by solving the Born-Markov master equation [10,11], given by

$$\frac{d\rho}{dt} = \frac{1}{i\hbar}[H_{AC}, \rho] + \mathcal{L}[\rho], \tag{3}$$

for upper $|F_u, M_{F_u}\rangle$ and lower $|F_l, M_{F_l}\rangle$ levels of the clock transition. Here, the total Hamiltonian of the system is given by $H_{AC} = H^0_{AC} + H^I_{AC}$ with the unperturbed Hamiltonian

$$H^0_{AC} = \sum_{j=1}^{N_a} \left(\frac{\hbar\omega_a}{2}\hat{\sigma}^z_j + \hbar\omega_c \hat{a}^\dagger_c \hat{a}_c \right)$$

and the interaction Hamiltonian

$$H^I_{AC} = \frac{\hbar g}{2} \sum_{j=1}^{N_a} (\hat{a}^\dagger_c \hat{\sigma}^-_j + \hat{a}^-_c \hat{\sigma}^\dagger_j).$$

In these expressions, ω_a is the angular frequency of the clock transition, ω_c is the angular frequency of the cavity mode, $\hat{\sigma}^z_j = |F^j_u, M^j_{F_u}\rangle\langle F^j_u, M^j_{F_u}| - |F^j_l, M^j_{F_l}\rangle\langle F^j_l, M^j_{F_l}|$, $\hat{\sigma}^-_j = (\hat{\sigma}^\dagger_j)^\dagger = |F^j_u, M^j_{F_u}\rangle\langle F^j_l, M^j_{F_l}|$, the atom-cavity coupling constant $g = \mu\sqrt{\frac{8\pi\omega_a}{\hbar\varepsilon_0 V_c}} = 4.09 \times 10^6$ Hz for the actual $E1$ matrix element μ of the clock transition and cavity mode volume V_c, and $\mathcal{L}[\rho]$ is the net Liouvillian containing contributions from the cavity, spontaneous decay, pumping laser, and inhomogeneous lifetime of the upper state. The output power of the bad-cavity is estimated as $P = \hbar\omega_a\kappa\ |\mathrm{tr}[\rho_{cw} a_c]|^2$ for the steady-state solution ρ_{cw} of the above equation and cavity dissipation rate κ. The estimated steady-state output power of the superradiant lasing is $P = 24\ \mu$W for a typical $N_a = 10^7$ atoms achieved through population-inversion with the pumping and repumping laser intensities of 500 and 2 mW/cm^2, respectively.

The quantum restricted linewidth $\Delta\upsilon$, following the modified Schawlow-Townes formula for a bad cavity, is given by [12]

$$\Delta\upsilon = \frac{\hbar\omega_a\kappa^2}{4\pi P} N_{sp} \left(1 + \left[\frac{2(\omega_c - \omega_a)}{\Gamma_u + \kappa}\right]^2\right)\left(\frac{\Gamma_u}{\Gamma_u + \kappa}\right)^2, \tag{4}$$

where $N_{sp} = \rho_u/(\rho_u - \rho_l)$ with ρ_u and ρ_l being the atomic population densities in the upper and lower states, and Γ_u is the spontaneous decay rate of the clock transition. We have set the cavity dissipation rate as $\kappa = 100\ \Gamma_u$. The quantum-limit linewidth of the superradiant lasing is anticipated to be narrowed down to 4.2 mHz for the 5.5% and 0.6% population densities in the upper and lower levels of the clock transition, respectively.

Typical orders of magnitudes of the major systematics to the clock frequency due to blackbody radiation (BBR) shifts, light shifts caused by the pumping and repumping lasers, and second-order Zeeman shifts, are determined by using the scalar ($\alpha_F^{E1(0)}$) and tensor ($\alpha_F^{E1(2)}$) $E1$ polarizabilities and magnetic dipole ($M1$) polarizabilities (α_F^{M1}) of the hyperfine levels that are listed in Table II. Using the differential static scalar $E1$ polarizabilities, $\delta\alpha_F^{E1(0)}(0)$ between the $|7S_{1/2}; F = 4, M_F = 0\rangle$ and $|6P_{3/2}; F = 3, M_F = 0\rangle$ clock levels, the BBR shift at room temperature (300 K) is determined by

$$\delta E^{E1}_{\mathrm{BBR}} = -\frac{1}{2}(831.9\,\mathrm{V/m})^2\left[\frac{T(\mathrm{K})}{300}\right]^4 \delta\alpha_F^{E1(0)}(0). \tag{5}$$

The fractional BBR shift in the clock frequency is estimated to be $1.94(2) \times 10^{-13}$. This uncertainty can be suppressed by two more orders by measuring the differential scalar $E1$ polarizability of the clock transition more precisely and conducting the experiment at a lower temperature. The light shifts due to the pumping and repumping lasers lead to the fractional clock frequency shifts $-1.6(7) \times 10^{-14}$ and $-1.8(1) \times 10^{-15}$, respectively. Since powers of these lasers can be controlled with an instability below 10^{-4} [33,34], it is possible to curtail the above fractional uncertainties to the 10^{-18} level. The choice of the $M_F = 0 \to M_F = 0$ clock transition gives zero first-order Zeeman shift. The second-order Zeeman shift of a hyperfine level is estimated by $\Delta E^{2^{\mathrm{nd}}}_{\mathrm{Zeeman}} = -\frac{1}{2}\alpha_F^{M1}\mathcal{B}^2$. The fractional shift in the clock frequency due to this effect is estimated from the difference of α_F^{M1} values, which is determined as

$$\alpha_F^{M1} = -\frac{2}{3(2F+1)} \sum_i \frac{|\langle F||O^{M1}||F_i\rangle|^2}{E_F - E_{F_i}}$$

for $M1$ operator O^{M1} and all possible F_i levels of the clock states with energies E_{F_i}. Uncertainties in these quantities come mainly from the energies. The α_F^{M1} values of the $|7S_{1/2}; F = 4, M_F = 0\rangle$ and $|6P_{3/2}; F = 3, M_F = 0\rangle$ levels are found to be -1.4×10^4 and -2.6×10^5 a.u., respectively. This gives a negligibly small fractional second-order Zeeman shift to the clock frequency. Other systematical effects are expected to be much less than the 10^{-15} level.

In summary, we have proposed a continual superradiant lasing scheme to construct an active lattice clock based on optical lattices. A suitable magic wavelength of the $|7S_{1/2};$

TABLE II. Scalar and tensor components of $E1$ polarizabilities (in a.u.), and $M1$ polarizabilities (in a.u.) of the clock levels. Estimated fractional shifts in the clock frequency from various systematics using the above quantities are listed in the bottom part.

Properties	$\lvert 7S_{1/2}(F=4)\rangle$	$\lvert 6P_{3/2}(F=3)\rangle$
$\alpha_F^{E1(0)}(0)$	6238(15)	1647(35)
$\alpha_F^{E1(0)}$(455 nm)	82(3)	−54(24)
$\alpha_F^{E1(0)}$(894 nm)	−267(11)	−4129(111)
$\alpha_F^{E1(2)}$(455 nm)	0	−3(1)
$\alpha_F^{E1(2)}$(894 nm)	0	1679(25)
α_F^{M1}	$-1.4(1) \times 10^4$	$-2.6(2) \times 10^5$
Fractional frequency shifts		
BBR static at 300 K		$1.94(2) \times 10^{-13}$
455 nm laser, $I = 500$ mW/cm^2		$-1.6(7) \times 10^{-14}$
894 nm laser, $I = 2$ mW/cm^2		$-1.8(1) \times 10^{-15}$
2$^{\mathrm{nd}}$ Zeeman, $\mathcal{B} = 10^{-7}$ T		$-7.1(3) \times 10^{-19}$

$F = 4, M_F = 0\rangle \rightarrow |6P_{3/2}; F = 3, M_F = 0\rangle$ clock transition of Cs atoms has been narrowed down to confine atoms strongly in the optical lattices with densely populated ground and excited states. By simulating realistic experimental conditions, we predict to achieve a fractional uncertainty in the clock frequency of about 10^{-15} and a linewidth of a few mHz. Its bad-cavity operational mode can provide a robust short-term stability to this active clock. This, in combination with another high-accuracy passive optical clock, can be used to create better short- and long-term stabilities for practical applications.

The work was supported by National Natural Science Foundation of China (NSFC) (Grants No. 91436210 and No. 11874064) and the Strategic Priority Research Program of the Chinese Academy of Sciences (CAS), Grant No. XDB21030300, and the NKRD Program of China, Grant No. 2016YFA0302104. The work of B.A. is supported by DST-SERB (India) Grant No. EMR/2016/001228. B.K.S. thanks IOP, Beijing for the overseas professor fellowship and the hospitality to carry out this work. D.P and J.B.C. acknowledge valuable discussions with F. Fang.

[1] D. G. Matei, T. Legero, S. Häfner, C. Grebing, R. Weyrich, W. Zhang, L. Sonderhouse, J. M. Robinson, J. Ye, F. Riehle, and U. Sterr, Phys. Rev. Lett. **118**, 263202 (2017).

[2] T. Kessler, C. Hagemann, C. Grebing, T. Legero, U. Sterr, F. Riehle, M. J. Martin, L. Chen, and J. Ye, Nat. Photonics **6**, 687 (2011).

[3] W. Zhang, J. M. Robinson, L. Sonderhouse, E. Oelker, C. Benko, J. L. Hall, T. Legero, D. G. Matei, F. Riehle, U. Sterr, and J. Ye, Phys. Rev. Lett. **119**, 243601 (2017).

[4] T. L. Nicholson, S. L. Campbell, R. B. Hutson, G. E. Marti, B. J. Bloom, R. L. McNally, W. Zhang, M. D. Barrett, M. S. Safronova, G. F. Strouse, W. L. Tew, and J. Ye, Nat. Commun. **6**, 6896 (2015).

[5] R. Yanagimoto, N. Nemitz, F. Bregolin, and H. Katori, Phys. Rev. A **98**, 012704 (2018).

[6] J.-S. Chen, S. M. Brewer, C. W. Chou, D. J. Wineland, D. R. Leibrandt, and D. B. Hume, Phys. Rev. Lett. **118**, 053002 (2017).

[7] N. Huntemann, C. Sanner, B. Lipphardt, Chr. Tamm, and E. Peik, Phys. Rev. Lett. **116**, 063001 (2016).

[8] A. Golovizin, E. Fedorova, D. Tregubov, D. Sukachev, K. Khabarova, V. Sorokin, and N. Kolachevsky, Nat. Commun. **10**, 1074 (2019).

[9] S. Sonar, M. Hajdusek, M. Mukherjee, R. Fazio, V. Vedral, S. Vinjanampathy, and L. C. Kwek, Phys. Rev. Lett. **120**, 163601 (2018).

[10] D. Meiser, J. Ye, D. R. Carlson, and M. J. Holland, Phys. Rev. Lett. **102**, 163601 (2009).

[11] G. A. Kazakov and T. Schumm, Phys. Rev. A **95**, 023839 (2017).

[12] S. J. M. Kuppens, M. P. van Exter, and J. P. Woerdman, Phys. Rev. Lett. **72**, 3815 (1994).

[13] M. A. Norcia, J. R. K. Cline, J. A. Muniz, J. M. Robinson, R. B. Hutson, A. Goban, G. E. Marti, J. Ye, and J. K. Thompson, Phys. Rev. X **8**, 021036 (2018).

[14] T. Laske, H. Winter, and A. Hemmerich, Phys. Rev. Lett. **123**, 103601 (2019).

[15] D. Yu and J. Chen, Phys. Rev. Lett. **98**, 050801 (2007).

[16] D. Pan, T. Shi, and J. Chen, IEEE Trans. Ultrson. Ferroelectr. Freq. Control **65**, 1958 (2018).

[17] G. Avila, E. De Clercq, M. Labachellerie, and P. Cérez, IEEE Trans. Instrum. Meas. **IM-34**, 139 (1985).

[18] S. Singh, B. K. Sahoo, and B. Arora, Phys. Rev. A **93**, 063422 (2016).

[19] S. Singh, K. Kiranpreet, B. K. Sahoo, and B. Arora, J. Phys. B: At., Mol. Opt. Phys. **49**, 145005 (2016).

[20] G. Toh, A. Damitz, C. E. Tanner, W. R. Johnson, and D. S. Elliott, Phys. Rev. Lett. **123**, 073002 (2019).

[21] A. Damitz, G. Toh, E. Putney, C. E. Tanner, and D. S. Elliott, Phys. Rev. A **99**, 062510 (2019).

[22] G. Toh, A. Damitz, N. Glotzbach, J. Quirk, I. C. Stevenson, J. Choi, M. S. Safronova, and D. S. Elliott, Phys. Rev. A **99**, 032504 (2019).

[23] M. S. Safronova and W. R. Johnson, Adv. At. Mol. Opt. Phys. **55**, 191 (2008).

[24] P. Lett, W. Phillips, and S. Rolston, J. Opt. Soc. Am. B **6**, 2084 (1989).

[25] J. Dalibard and C. Cohen-Tannoudji, J. Opt. Soc. Am. B **6**, 2023 (1989).

[26] J. Dalibard, S. Reynaud, and C. Cohen-Tannoudji, J. Phys. B: At. Mol. Phys. **17**, 4577 (1984).

[27] J. Hou, Y. Li, D. Yang, and Y. Wang, Acta Phys. Sin. (Overseas Edn) **7**, 881 (1998).

[28] A. Derevianko and H. Katori, Rev. Mod. Phys. **83**, 331 (2011).

[29] M. M. Boyd, Ph.D thesis, University of Colorado, 2007 (unpublished).

[30] M. O. Scully and M. S. Zubairy, *Quantum Optics* (Cambridge University Press, Cambridge, England, 1997).

[31] D. A. Steck, Cesium D Line Data, http://steck.us/alkalidata (2010).

[32] A. Kramida, Y. Ralchenko, J. Reader, and NIST ASD Team, NIST Atomic Spectra Database, https://physics.nist.gov/asd

[33] R. Lin, D. Liu, J. Ruan, W. Zhao, and X. Wang, in *Proceedings of 2014 IEEE International Frequency Control Symposium (FCS)Taipei, Taiwan* (IEEE, Piscataway, NJ, 2014), pp. 19–22.

[34] F. Tricot, D. H. Phung, M. Lours, S. Guerandel, and E. De Clercq, Rev. Sci. Instrum. **89**, 113112 (2018).